INTERNATIONAL JOURNAL OF CLIMATOLOGY
Int. J. Climatol. **36**: 1278–1290 (2016)
Published online 28 July 2015 in Wiley Online Library
(wileyonlinelibrary.com) DOI: 10.1002/joc.4423

RMetS
Royal Meteorological Society

Agro-climate changes over Northeast Asia in RCP scenarios simulated by WRF

Joong-Bae Ahn,[a] Ja-Young Hong[a]* and Kyo-Moon Shim[b]
[a] *Division of Earth Environmental System, Pusan National University, South Korea*
[b] *Division of Climate Change and Agroecology, National Academy of Agricultural Science, Wanju, South Korea*

ABSTRACT: Dynamically downscaled agro-climates for present (1981–2010) and future (2071–2100) climates under Representative Concentration Pathways (Historical, RCP4.5, and RCP8.5) in Northeast Asia (118°–138°E, 30°–45°N) are analysed in terms of the indices, such as vegetable and crop periods, frost days, and the climatic yield potential (CYP) for Japonica type rice (hereafter, rice). The model employed for dynamical downscaling is the Weather Research and Forecasting (WRF), with a 12.5-km horizontal grid spacing in the domain. According to our results, the CYP for rice, one of the major crops presently cultivated in the area, is expected to decrease throughout most of the region, despite a projected expansion of both vegetable and crop periods. This is projected to occur particularly in South Korea, Japan, and Southeast and Northeast China. Such a change is related to the projected rise in temperature within these regions, which will exceed the grain-filling optimum temperature of rice. In contrast, the climate projection of the RCPs is that the CYP will increase over northeastern parts of the Korean Peninsula and the Russian Far Eastern region (Primorsky), because temperatures in these regions are expected to rise and approach the grain-filling optimum temperature. For the RCPs, the optimum heading date, on which the domain averaged CYP is the highest, is expected to be later than that of the Historical by approximately 17–24 days. In addition, the maximum CYP in the RCPs is projected to decrease compared with that of the historical, and the possible period of rice ripening (period in which the CYP is greater than 0) is also expected to decrease.

KEY WORDS climate change; RCPs; Northeast Asia; CYP; agro-climate index; Japonica type rice

Received 29 September 2014; Revised 28 May 2015; Accepted 28 May 2015

1. Introduction

According to the Fifth Assessment Report of the Intergovernmental Panel on Climate Change (IPCC), global mean surface air temperature has risen by 0.89 °C over the last century (1901–2012) because of the augmentation of greenhouse gases such as CO_2, and the rate of warming has been rapidly increasing since the 1950s (globally 0.01 °C year^{-1}). Increased greenhouse gases have caused changes in the weather and climate, and accordingly have influenced subsystems on Earth, such as the biosphere. Such changes have led to serious food security risks for countries over the entire globe (Australian Agency for International Development, 2004; U.S. Government, 2010; Alexandratos and Bruinsma, 2012), and the United Nations Framework Convention on Climate Change has formally recognized that climate change will seriously impact agriculture (Su *et al.*, 2009). The Organisation for Economic Co-operation and Development–Food and Agriculture Organization (2013) expects that international prices of major crops (e.g., wheat, oilseeds, rice, coarse and raw sugar, and grains) and livestock products will rise over the next decade owing to the slower growth in production, together with other causes such as the use of crops for energy and biofuels, which will exacerbate food shortages. Thus, it is necessary for each country to consider any issues in relation to their ability to maintain their populations by being self-sufficient. This is of considerable importance in Northeast Asia, as the region hosts about 20% of the world's population (Central Intelligence Agency, 2014).

On the basis of results from climate change scenarios with a coupled general climate model, Meehl *et al.* (2004) stated that throughout the 21st century in the United States the number of frost days will decrease in accordance with changes in night-time minimum temperatures. In addition, Bonsal *et al.* (2001) and Heino *et al.* (1999) displayed similar results for Canada and Northern Europe, respectively. Frich *et al.* (2002) calculated growing season length (GSL), which is defined as the number of days in which the daily mean temperature is higher than 5 °C, and found that the GSL had lengthened throughout most of the mid-latitudes in the Northern Hemisphere. Shim *et al.* (2008) divided data for the period 1969–2006 into two different intervals, and using the agro-climatic index showed that vegetable and crop growth periods on the Korean Peninsula have increased. However, Lal *et al.* (2005) reported that while an increased concentration of atmospheric CO_2 normally improves crop productivity, the

* Correspondence to: J.-Y. Hong, Department of Atmospheric sciences, Pusan National University, 2, Busandaehak-ro 63beon-gil, Geumjeong-gu, Busan, 609-735, South Korea. E-mail: hongja0627@pusan.ac.kr

current yield of rice in tropical regions will decrease by 17% in case of a temperature rise of 2 °C. Gao (2012) insisted that by the 2030s, crop production in China will also be reduced if sufficient adaptation measures are not taken.

Several recent studies have compiled agricultural projections based on the Coupled Model Intercomparison Project phase 5 (CMIP5) (Taylor *et al.*, 2012) model data. Using future climate data from CMIP phase 3 (CMIP3) (Meehl *et al.*, 2007) and CMIP5, Sultan *et al.* (2013) considered that millet and sorghum yields in West Africa would decrease by 0–41% at the end of the 21st century, mainly because of temperature rises. Ramirez-Villegas *et al.* (2013) simulated temperature thresholds for 12 major crops (including wheat, maize, rice, barley, soybean, cassava, and potato) in the Andes, Africa, and South Asia using a crop model based on raw CMIP3 and CMIP5 data (data without model bias treatment). Results showed that the root mean square errors (RMSEs) of temperature in CMIP5 decreased in comparison with those of CMIP3, except for winter precipitation. Therefore, the authors suggested that the data produced based on CMIP5 were more realistic than the CMIP3 data.

The objective of the study is to estimate climatic rice production changes for the future climate in terms of the agro-climate indices over Northeast Asia, using dynamically downscaled data forced by CMIP5 simulations. For these objectives, we used a coupled general circulation model (CGCM) data of CMIP5 based on Representative Concentration Pathways (RCPs) (Moss *et al.*, 2008; van Vuuren *et al.*, 2011). Furthermore, we applied a dynamical downscaling method with a horizontal resolution of 12.5 km to produce the regional climate in Northeast Asia (118°–138°E, 30°–45°N) and simulate the regional climate in detail, using CGCM data for the boundary and initial conditions of the regional climate model, Weather Research and Forecasting (WRF).

The models and observations used in this paper, and the experimental design are introduced in Section 2. Section 3 then analyses the simulation performance of the WRF in terms of the agro-climate, and Section 4 presents the agro-climate changes under RCP scenarios. Summary and conclusions are finally presented in Section 5.

2. Model and data

2.1. Model experiment and data

In this study, the WRF version 3.4 (Skamarock *et al.*, 2008), a community mesoscale numerical weather prediction system, is employed as a regional climate model. The WRF model adopts a fully compressible and non-hydrostatic assumption, and a terrain-following hydrostatic pressure coordinate. A general explanation of the model can be found at http://www.wrf-model.org/index.php.

Initial and boundary forcing data for dynamic downscaling are obtained from the Hadley Centre Global Environmental Model version 2 – Atmosphere and Ocean (HadGEM2-AO) results, produced by National Institute of Meteorological Research/Korea Meteorological Administration (NIMR/KMA). The NIMR/KMA is jointly participating in the CMIP5 experiments with the Met Office Hadley Centre using HadGEM2-AO (Baek *et al.*, 2013). Baek *et al.* (2013) showed that HadGEM2-AO has fine performance in simulating the global warming and multi-decadal variation over India and the East Asia regions. The HadGEM2-AO simulations are based on the IPCC Historical, RCP4.5, and RCP8.5 scenarios (HS, RCP4.5, and RCP8.5 runs, respectively, hereafter). Spatial and temporal resolutions of the HadGEM2-AO data are 1.875° × 1.25° and 6 h, respectively. A detailed description of the model is provided in Collins *et al.* (2011) and Baek *et al.* (2013).

The WRF simulation domain covering Northeast Asia is centered on 127.5°E and 37.5°N, and has a 12.5 km horizontal resolution (Figure 1) with 28 vertical layers. The physical processes used in this study consist of the Kain-Fritsch cumulus parameterization (Kain, 2004), WRF Single-Moment 3-class microphysics (Hong *et al.*, 2004), the National Center for Atmospheric Research (NCAR) Community Atmospheric Model (CAM) longwave and shortwave radiation (Collins *et al.*, 2002), Monin–Obukhov similarity surface layer physics (Jiménez *et al.*, 2012), the Noah land surface model (Chen and Dudhia, 2001), and the Yonsei University planetary boundary layer physics (Hong *et al.*, 2006). In addition, yearly varying CO_2 concentrations (Meinshausen *et al.*, 2011) are applied, with an integration time step of 60 s. The configuration of the WRF used in this study is summarized in Table 1.

The WRF simulations were conducted from 1 January 1979 to 31 December 2010 for the HS run, and from 1 January 2019 to 31 December 2100 for the RCP4.5 and RCP8.5 runs. Simulation outputs were saved every hour over the entire simulation period. Two different analysis periods were chosen to examine the agro-climate during different climatic periods: 1981–2010 (the first 2 years

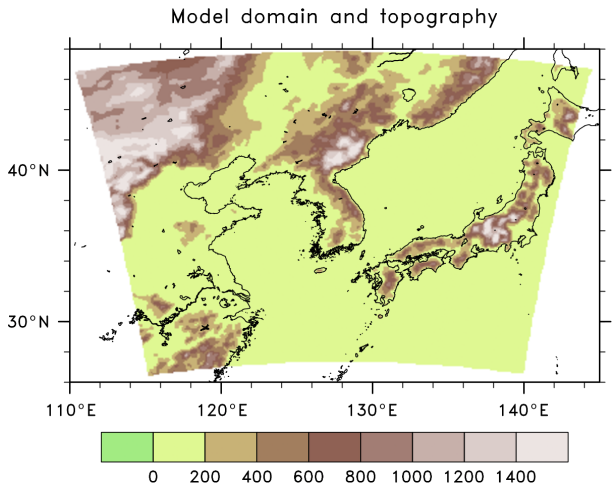

Figure 1. The domain and topography (m) of WRF.

Table 1. Physical schemes of the WRF and details of the model's configuration.

Contents	Description
Equation	Non-hydrostatic
Vertical levels (top)	28 (50 hPa)
Horizontal resolution	12.5 km
Domain dimensions	201×180
Integration time step	60 s
Microphysics scheme	WRF Single-Moment 3-class (Hong *et al.*, 2004)
Longwave/shortwave radiation	NCAR CAM (Collins *et al.*, 2002)
Surface layer	Monin-Obukhov similarity (Jiménez *et al.*, 2012)
Land surface process	Noah (Chen and Dudhia, 2001)
Planetary boundary layer	Yonsei University (Hong *et al.*, 2006)
Cumulus parameterization	Kain-Fritsch (Kain, 2004)

are considered as model spin-up time) for the current climate, and 2071–2100 for the future climate. The analysis variables used were daily mean surface air temperature, daily minimum temperature for frost days, hourly precipitation, and hourly incoming net shortwave radiation (SR). The daily duration of sunshine was calculated using hourly precipitation and SR. Specifically, each hour was accumulated as a daily duration of sunshine if hourly SR exceeds 0 and hourly precipitation equals 0 for each grid point.

Two sets of observation data with different horizontal resolutions were used to evaluate the simulated variables: $0.5° \times 0.5°$ horizontal resolution monthly temperature and frost days from the Climatic Research Unit (CRU) time series (TS) 3.2 (Harris *et al.*, 2014) for the period 1981–2010, and $0.25° \times 0.25°$ horizontal resolution daily temperature from the Asian Precipitation–Highly Resolved Observational Data Integration Towards Evaluation of Water Resources (APHRODITE) V1204R1 (Yasutomi *et al.*, 2011) for the period 1978–2007. However, although the horizontal resolution of the CRU is relatively lower than that of APHRODITE, the CRU provides frost days, whereas APHRODITE data (which contain higher spatial and temporal resolution data than CRU) do not provide minimum temperature, which means that frost days cannot be calculated. Therefore, frost days were compared to CRU data in the HS run, and other indices were compared to data calculated using APHRODITE data. In addition, the Student's *t*-test is performed to illustrate the statistical significance level of the model results.

As our major concern in this study is to investigate the future changes of agro-climate, systematic model biases have been removed in estimating the projected agro-climate changes by subtracting the results of the HS run from those of the RCP runs. The bias correction method used in this study has been widely used in many studies (e.g., Ahn *et al.*, 2012; Chen and Sun, 2013; Gao *et al.*, 2013; Oh *et al.*, 2014; Hong and Ahn, 2015).

2.2. Agro-climate indices

Frost occurs when the surface minimum temperature drops below 0 °C due to phenomena such as radiation cooling or cold temperature advection (Moonen *et al.*, 2002; Meehl *et al.*, 2004), and frost adversely affects crops by freezing cellular tissue and damaging foliage. In this study, frost days are defined as the number of days on which the daily minimum temperature is below 0 °C between September and March (SONDJFM), and the first and last frost dates are defined as dates on which a daily minimum temperature lower than 0 °C appeared first and last, respectively, during the SONDJFM period.

Many plants germinate or elongate when the daily mean temperature is 5 °C or higher (Shim *et al.*, 2008). The vegetable period is an indicator of the climatic limit in which cultivation can occur, and of periods that are suitable for the cultivation of overwintering crops such as barley and apple trees. It is defined as the number of days in which the daily mean temperature is above 5 °C from March to October (MAMJJASO).

The crop period for rice is an index that measures the number of days where the daily mean temperature is above 15 °C, which is a critical temperature for the rice rooting period. Rooting of rice seedlings under natural conditions is only possible when the temperature is at least 15 °C (Shim *et al.*, 2008). The crop period for rice are defined as the accumulated numbers of days on which the daily mean temperatures are at least 15 °C during the MAMJJASO period.

It is difficult to quantify regional climatic resources during the rice cultivation period. However, one possible way to evaluate them is to estimate the Climate Yield Potential (CYP), assuming that no unexpected agrometeorological disasters will occur during the cultivation period (Shim *et al.*, 2008). The index differs depending on the crop species. In this study, the CYP for the rice species Japonica type rice (hereafter, rice), the major crop grown in Korea, northeastern China, and Japan is estimated.

CYP of rice defined in terms of the grain-filling optimum temperature is obtained from average daily surface air temperature (T_1) and accumulated hours of sunshine (DS) during the 40-day after the heading date (Hanyu *et al.*, 1966):

$$\mathrm{CYP}\ \left(\mathrm{kg}\ 10^{-3}\ \mathrm{m}^{-2}\right) = \mathrm{DS}\left(\alpha - \beta\left(T_\mathrm{a} - T_1\right)^2\right) \quad (1)$$

where the α and β are regression coefficients, which can be changed depending on the variety of rice. T_1 is the most proper mean temperature for rice during the grain-filling period. In this study, α, β, and T_1 are assigned as 4.14, 0.13, and 21.4, respectively, following Hanyu *et al.* (1966). It is possible to consider that it may not be strictly relevant to apply this empirical formula to the whole domain, as the equation was deduced for use in the agricultural climate over Japan and all the various rice cultivars. However, it is considered that the domain where rice is mainly cultivated and which is used in this study is a relatively small area comprising the Korean Peninsula and some of Japan and

China, and we therefore assume that there will be no significant problem in estimating the indices with this formula. The constant threshold values in Equation (1) have also been used in many studies estimating CYP for rice in the Korean Peninsula (e.g., Son *et al.*, 2002; Kim *et al.*, 2007).

2.3. Experimental design

Because the CYP is obtained using the average temperature and accumulated sunshine hours over 40 days after rice heading, it is necessary to obtain a heading date. The optimum heading date period for rice cultivars in the central region of the Korean Peninsula is from early to late August (Shim *et al.*, 2008), and the average optimum seeding season for rice is from late April to late May (Lee *et al.*, 2012). The heading dates for rice in the southeastern and northeastern regions of China are from between 70.6 days and 109.3 days after seeding (Wei *et al.*, 2008; Wei *et al.*, 2009). Because the domain of this study includes the region around the Korean Peninsula, every day from 1 July to 18 September is defined as a heading date. That is, the earliest heading date of early maturing rice varieties seeded at the earliest day of optimum seeding season (21 April) becomes July 1 if the rice ears appear by 71 days (the shortest period for tillering and culm internode elongation) after seeding. Likewise, the latest heading date of late maturing rice varieties seeded at the last day of optimum seeding season (31 May) becomes September 18 if the rice ears appear by 110 days (the longest period for tillering and culm internode elongation) after seeding. Thus, in this study, the period from July 1 to September 18 is considered the heading date period for the rice.

3. Model performance for Historical climate

3.1. Surface air temperature

As surface air temperature is a major variable in the estimation of agro-climate indices, it is necessary to validate a climate reproducibility of the WRF model in terms of surface air temperature. To illustrate the general performance of the model, such as its ability to simulate general pattern and terrain-following fine distribution of surface air temperature, we presented the result from the HS run in Figure 2 without removing the bias. Figure 2(a) displays the simulated 30-year mean surface air temperature from the HS run over the domain, compared with the two observation data. The general pattern of surface air temperature over Northeast Asia is reproduced reasonably by the WRF. As the horizontal resolution of the WRF is higher than those of CRU and APHRODITE (Figure 2(b) and (c)), the fine distributions of temperature following terrain and altitude are better represented in the HS run. As in CRU and APHRODITE, climatological characteristics of latitudinal and altitudinal distribution are well simulated. For example, it is warmer in the western part of the Korean Peninsula than in the eastern part, in western Manchuria than in eastern Manchuria, and in the coastal area than the inland area over Japan, which is similar to the observations. The results of HS run basically show a cold bias over the domain, except for over the southern coastal region in Korea and Japan where there is a warm bias (Figure 2(d) and (e)). The eastern coast and northern (125°–132°E, 40°–45°N) regions of the Korean Peninsula have higher mountain ranges compared to other regions (Figure 1) and show relatively lower temperature distributions. However, CRU and APHRODITE data do not display detailed terrain-following temperatures because their spatial resolutions are relatively coarser compared with those of the HS run. The negative differences in these regions are attributable to differences in spatial resolutions between the data. As decreases in temperature according to altitude are reflected well in the high resolution data compared with the low resolution data, WRF simulated relatively low temperature distribution. That is, the higher the resolution, the greater the effect of elevation (Ahn *et al.*, 2012; Gerelchuluun and Ahn, 2014).

Table 2 displays scores of historical annual surface air temperature with respect to CRU (green) and APHRODITE (red) over the region. The pattern correlation coefficient of WRF with CRU (APHRODITE) and the normalized standard deviation of the model for CRU (APHRODITE) are close to 1.0. The root mean square errors (RMSEs) of the model do not present any large differences to those of the observation. Thus, the results indicate that the simulated surface air temperature in the HS run is similar to that of the observations in terms of magnitude, distribution, and spatial variation.

3.2. Agro-climate indices

Frost days as well as vegetable and crop periods for the HS run are compared with the results of CRU and APHRODITE in Figure 3. The latitudinal distribution and general pattern of the number of frost days in the HS run are similar to those from CRU (Figure 3(a)). The numbers of frost days in the HS run and from CRU are larger in the higher latitudes. Regionally, the number of frost days is smaller in the coastal area of Japan and in the southeastern region of China than in other regions, and those in the northern region of the Korean Peninsula are larger by at least 40 days than those in other regions on the same latitude. However, because of model bias and the difference in spatial resolutions between the CRU and the HS run, differences are seen in the number of frost days between the southwestern part of Korea and the northwestern part of Japan.

Both vegetable and crop periods for the HS run and APHRODITE are shorter in the northern part than in the southern area of the domain (Figure 3(b) and (c)). The vegetable and crop periods of the southeastern region of China, the southwestern coastal area of the Korean Peninsula, and the coastal area of Japan (areas which are warmer than other regions on the same latitude because of their lower altitudes) are longer than those of other regions, while those in the Liaoning region (119°–125°E, 39°–45°N) of China are similar to those of the central region of the Korean Peninsula which are situated on relatively lower latitudes. The vegetable periods of the

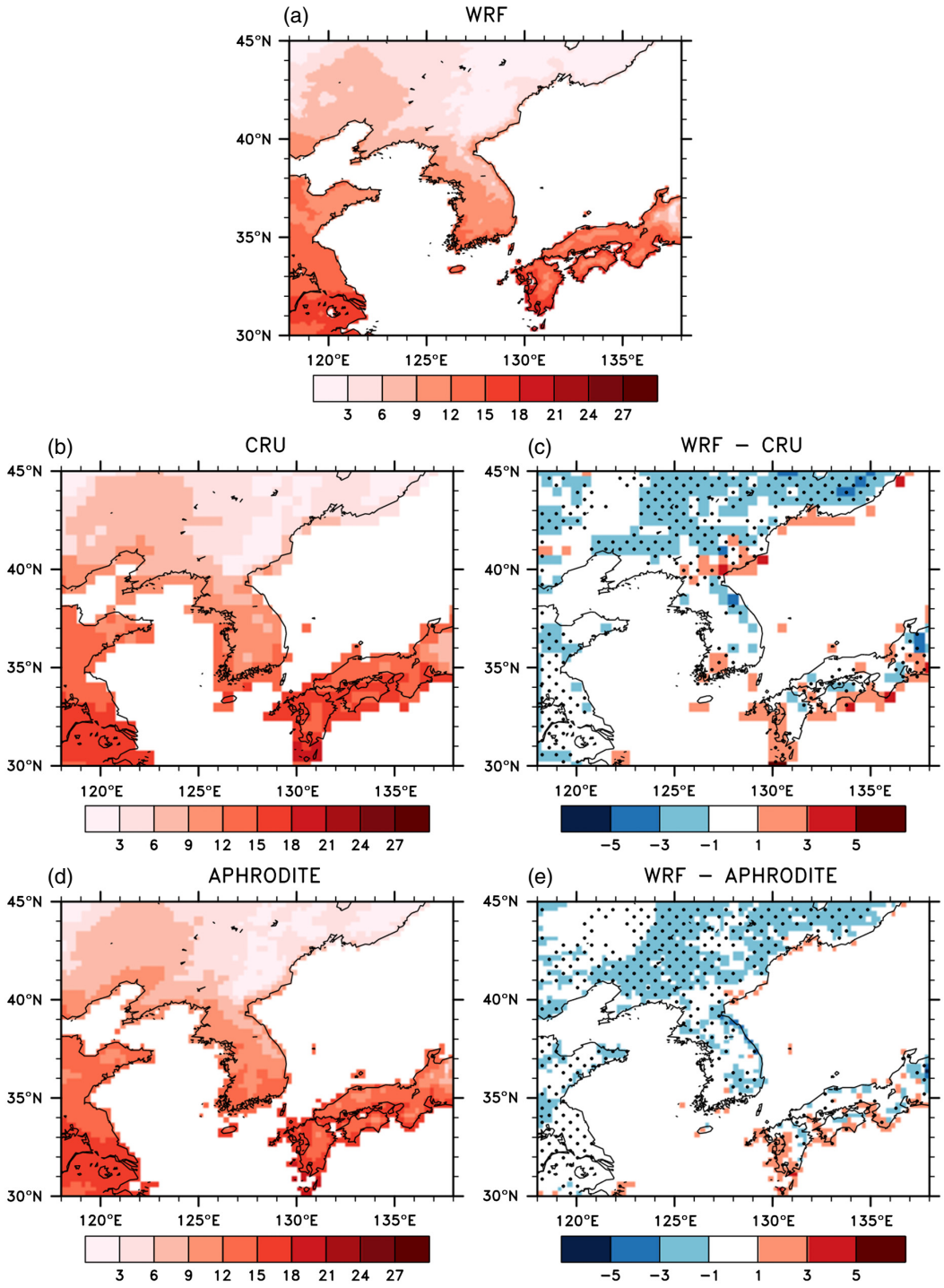

Figure 2. Distributions of annual mean surface air temperature from (a) HS run, (b) CRU, and (c) APHRODITE. Parts (d) and (e) show the differences between the HS run and each observation. The grid point with black dot shows the 95% confidence level based on the Student's *t*-test.

Table 2. Scores of annual mean surface air temperature averaged over Northeast Asia (118°–138°E, 30°–45°N) between the HS run and CRU (APHRODITE).

Versus HS run	Spatial correlations	Normalized standard deviations	RMSE
CRU	0.97	1.23	1.41
APHRODITE	0.99	1.10	1.14

HS run is similar to those of the APHRODITE, not only in terms of the patterns but also in the values produced. Therefore, there is less than 5 days difference between the two in most areas. The crop periods of the HS run shows negative differences in the coastal region of the Korean Peninsula, but positive differences in northeastern China and other parts of Korea. This is because the differences between the two are related to the model bias of the WRF and the difference in spatial resolution between the model

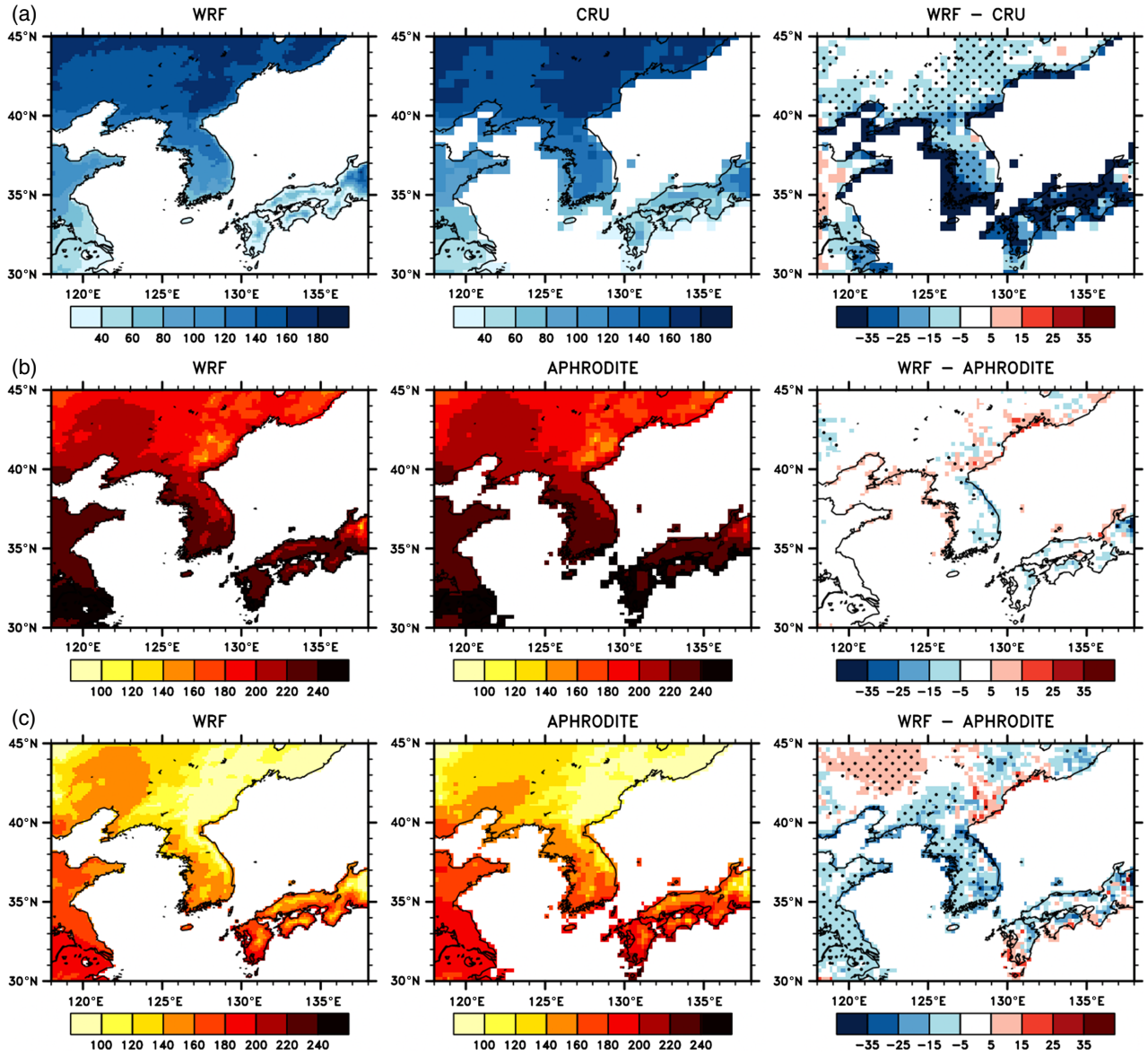

Figure 3. Averages (two left panels), and differences (right-most panels) of (a) SONDJFM frost days, (b) MAMJJASO vegetable periods, and (c) MAMJJASO crop periods for the HS run and observations. The grid point with black dot shows the 95% confidence level based on Student's *t*-test.

and the APHRODITE data. However, the general patterns of the crop periods in the model are quite similar to those in the APHRODITE data.

4. Agro-climate changes under RCP runs

4.1. Changes in temperature

Projected future changes in annual mean and minimum temperatures between the RCP runs and the HS run are shown in Figure 4. There is a significant increase in both variables for each RCP run. Relatively larger increases of mean and minimum temperatures at high latitude and high altitude regions are simulated for each case and RCP run. The increase in minimum temperature is greater compared with mean temperature. Overall, these changes are more substantial in the RCP8.5 run than in the RCP4.5 run. Regional mean temperature changes for mean and minimum temperature under the RCP4.5/RCP8.5 runs are 3.2 °C/5.3 °C and 3.5 °C/5.6 °C, respectively. The increases in mean and minimum temperature for the RCP4.5/RCP8.5 runs are usually less than 3.0 °C/4.5 °C and 3.0 °C/5.0 °C below 38°N, respectively. The largest warming in the RCP4.5/RCP8.5 runs, exceeding 3.5 °C/6.0 °C, respectively, was found in regions above 42°N.

4.2. Changes in frost, vegetable, and crop periods

Changes in the number of frost days under future climate changes are obtained from the difference between the RCP runs and the HS run for the two 30-year periods (Figure 5). The date of the first frost in fall is projected to be delayed by about 10–15 days in the RCP4.5 run, and by about 20–25 days in the RCP8.5 run within the domain. However, relatively larger retreat in the first frost

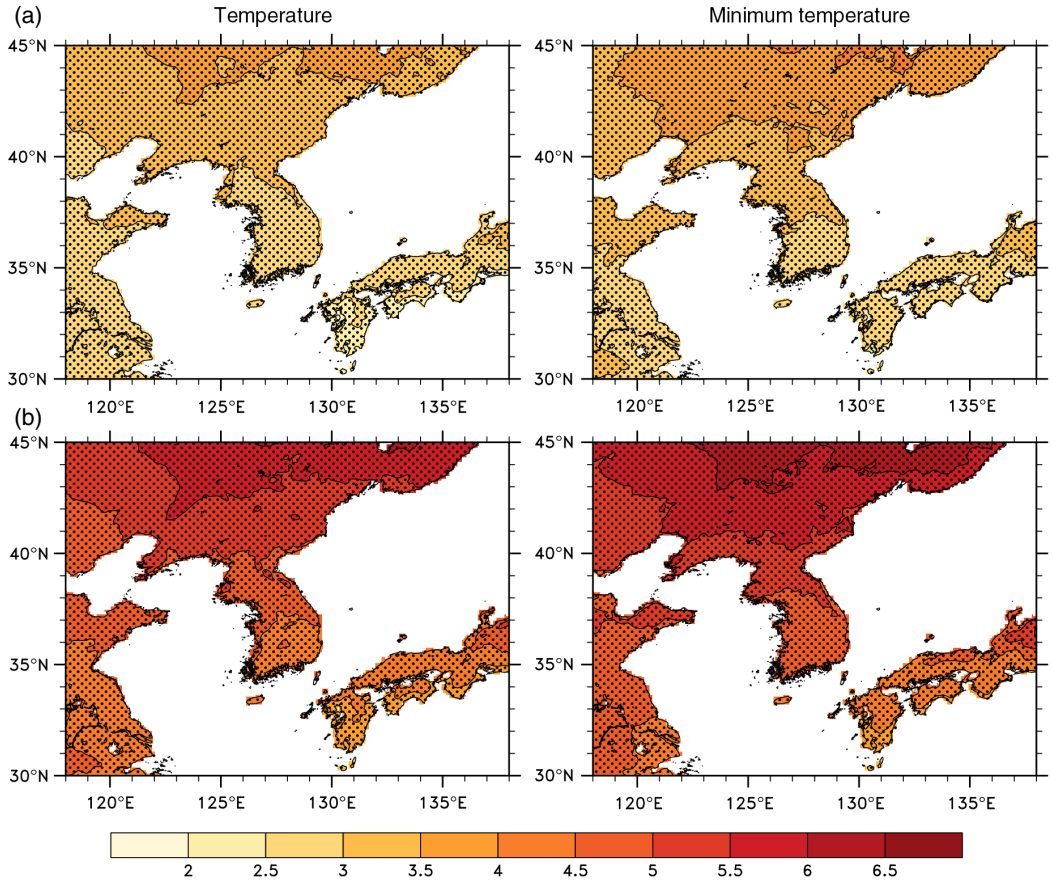

Figure 4. Changes in annual mean and minimum temperatures for (a) RCP4.5 and (b) RCP8.5 runs. Grid points with black dots show the 95% confidence level based on the Student's *t*-test.

date are projected in the southern part of the domain, where according to differences in the last frost dates during early spring, they are simulated to advance by 5–35 days. In general, a greater decrease is projected in the climate of the RCP8.5 run (by an average of 30 days) than in the RCP4.5 run (by an average of 20 days), with no increase seen throughout the entire region. In addition, for regions of lower latitude (below 38°N), a decrease of more than 30 days and 40 days is projected, respectively, for the RCP4.5 and RCP8.5 runs. These decreases in frost days are consistent with the previous studies of Sillmann *et al.* (2013) and Yang *et al.* (2014). They showed that the linear change of CMIP5 multi-model ensemble for frost days under RCP8.5 is about −40 days over East Asia and −46.9 days over China, respectively, by the end of the 21st century.

The vegetable periods throughout MAMJJASO are shown to increase by 5–15 days and by 10–35 days, for the RCP4.5 and RCP8.5 runs, respectively (Figure 6). The regions where the vegetable period is indicated to increase the most are the northeastern region of Korea and the central region of Japan and the values are larger in the RCP8.5 run than in the RCP4.5 run. No significant changes are projected over eastern China (30°–35°N) in either of the RCP runs.

The 30-year mean crop periods in MAMJJASO are projected to increase by at least 10 days in both the RCP runs (Figure 7). In the RCP climates, crop periods are projected to greatly increase in the central and northern regions of the Korean Peninsula, the inland region of Japan, and the Primorsky area (Far Eastern region) of Russia, where annual mean temperatures are relatively lower than in the southeastern region of China where annual mean temperatures are at least 12 °C (Figure 2(a)). The RCP4.5 run indicates a region where the crop period will be greater than 40 days, and this is situated along the eastern part of coastal region of the Korean Peninsula. This period rises to about 45 days over most of Korea in the RCP8.5 run, and the least differences are shown to be located in northeastern China. These are similar to the results obtained by Xia *et al.* (2015), who suggested that in the Northern Hemisphere by 2080–2099 relative to 1985–2004, the average number of days by which the start of the growing season advances based on CMIP5 models is about −11.3 days and −21.6 days under RCP4.5 and RCP8.5, respectively. Therefore, in comparison with the HS run, the number of frost days is decreased whereas, the vegetable and crop periods are increased, which suggests that the rice growing period will be increased.

4.3. Climatic yield potential (CYP)

4.3.1. CYP versus *heading dates*

Time series of domain-averaged CYPs for the HS, RCP4.5, and RCP8.5 runs with respect to heading dates

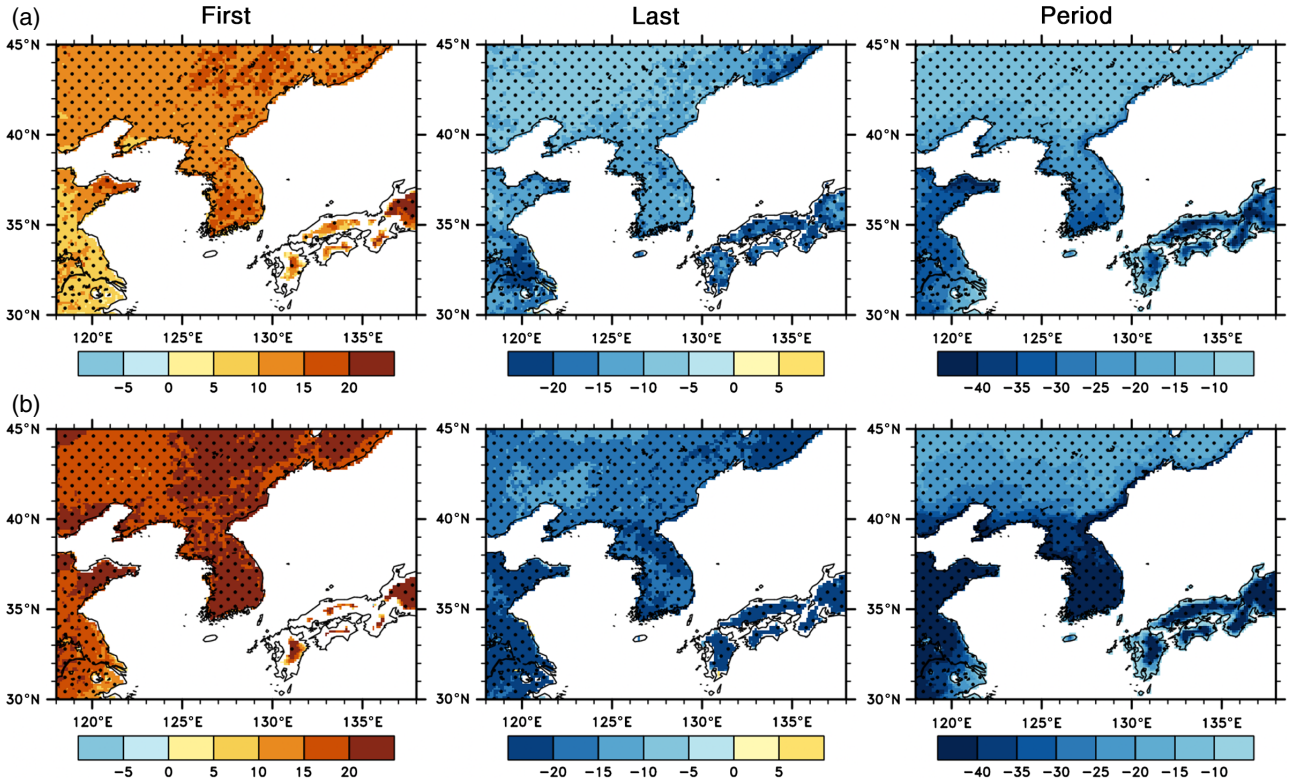

Figure 5. Changes in the first frost date in September–November, the last frost date in January–March, and frost days in September–March under the (a) RCP4.5 and (b) RCP8.5 runs. Grid points with black dots shows the 95% confidence level based on the Student's *t*-test.

are illustrated in Figure 8. The black, blue, and red solid lines indicate CYPs in the HS, RCP4.5, and RCP8.5 runs, respectively. The value at the vertical axis in Figure 8 is a CYP corresponding to the heading date. As mentioned earlier, for example, the CYP for a heading date of August 1 is determined by the temperatures and sunshine for 40 days from 2 August to 10 September. The CYP with the greatest value will deliver the largest production of rice, and but when the index is below 0, no rice has been produced. For instance, if the heading date is 1 August and the corresponding value of CYP is positive, temperatures and sunlight that are suitable for the ripening of rice are given for 40 days from 2 August. In addition, if the CYP of 1 August is larger than that of 1 July, 40 days from 2 August are considered a more appropriate grain-filling period than 40 days from July 2.

The CYP of the HS run (CYP-HS, hereafter) exhibiting high positive values when the heading dates are in early July gradually increases with later heading dates to reach its peak (1075) on a heading date of 4 August. The CYP-HS rapidly decreases with heading dates that are later than the middle of August, and reaches below 0 with heading dates later than 30 August. This means that the optimum heading dates in the CYP-HS are between early July and late August, and the result showing that the CYP is at its maximum when the heading date is in early August is similar to that of Shim *et al.* (2008). Therefore, the HS run appears to appropriately simulate the CYP from a temporal viewpoint.

The CYP of the RCP4.5 run (CYP-RCP4.5) reaches a value higher than 0 when the heading date is later than 15 July, and reaches its maximum (985) when the heading date is 21 August. It decreases with heading dates later than 21 August, and becomes 0 when the heading date is later than 12 September. The CYP of the RCP8.5 run (CYP-RCP8.5) shows zero rice productivity when the heading date occurs before early August, and only becomes positive when the heading date is later than 5 August showing a maximum (839) with a heading date of 28 August. It decreases when the heading date is later than 28 August, and reaches 0 when the heading date occurs later than 18 September.

These results imply that the maximum values of the CYP-RCPs are smaller than those of the CYP-HS, and that the maximum rice potential will therefore decrease in RCP climates. The number of days during which the CYP is at least 0 in the HS, RCP4.5, RCP8.5 runs is 61, 59, and 43 days, respectively. Therefore, the averaged CYP during which the value of CYP is above 0 is much smaller in the case of the CYP-RCP4.5 (588) and the CYP-RCP8.5 (543) compared with the CYP-HS (860). The smaller number of days in which the CYP is at least 0 is associated with disadvantages in cultivating rice that have diverse growth periods including early or late maturing cultivars. That is, if the number of days during which the CYP is at least 0 in the CYP-RCPs becomes smaller than that of the CYP-HS, cultivating the diverse rice that are currently cultivated will become difficult. In summary, the possible period of rice ripening and the average rice productivity is

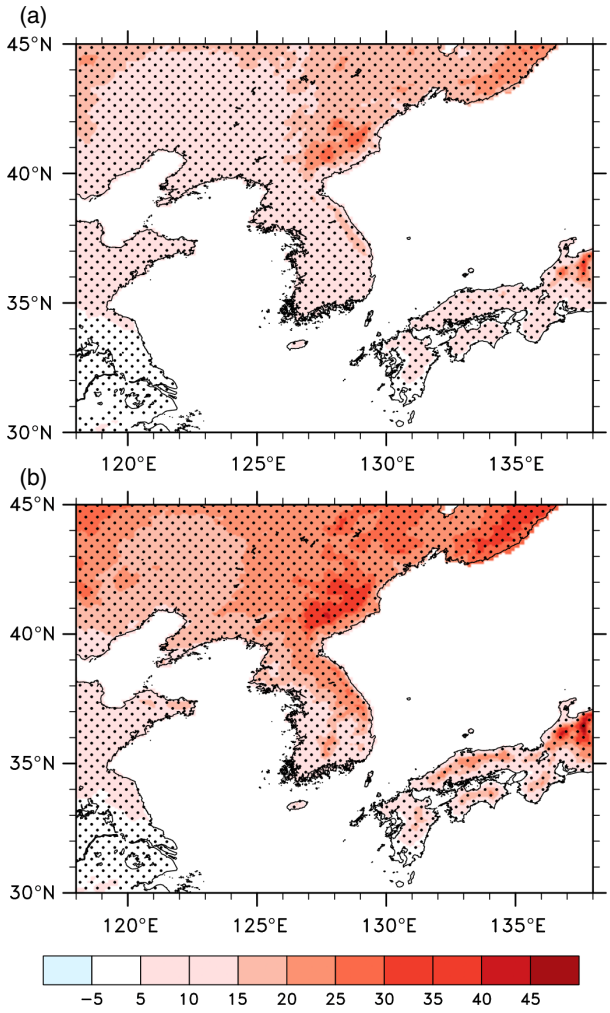

Figure 6. Vegetable period changes in March–October of (a) RCP4.5 and (b) RCP8.5 runs. Grid points with black dots show the 95% confidence level based on the Student's *t*-test.

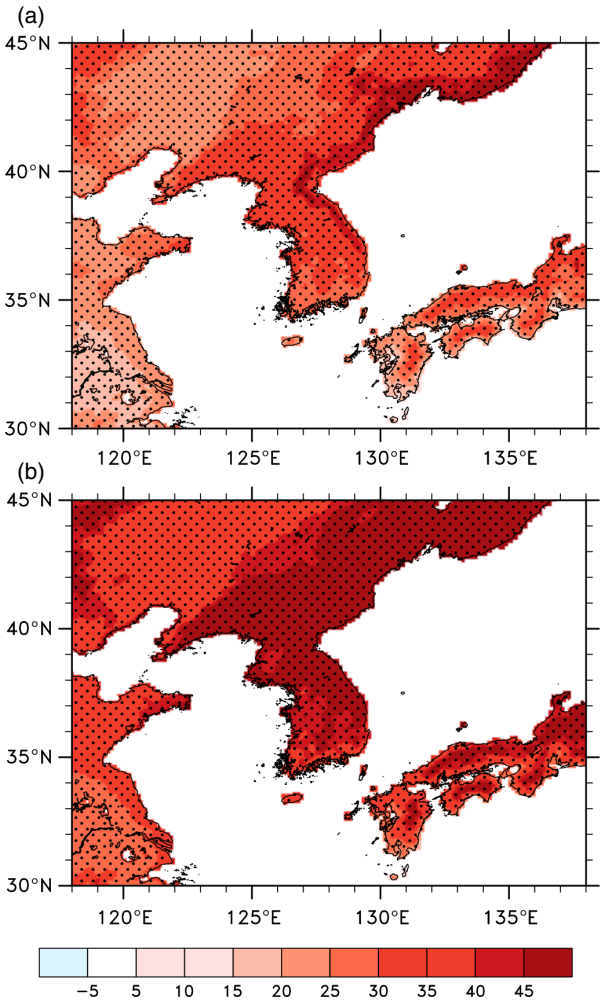

Figure 7. Same as Figure 6 except for the crop period.

shown to greatly decrease in the RCP runs compared with production in the HS run.

The domain average optimum grain-filling periods for rice in the RCP4.5 and RCP8.5 runs are from mid/late August to late September and from late August to early October, respectively. These periods are later by approximately 17 days and 24 days, respectively, compared with the HS run which shows dates from early August to the middle of September.

4.3.2. Spatial distribution of CYP changes

In this section, spatial changes in the CYP of the RCP runs are examined. The systematic model biases of the projected changes of the CYP have also been removed by subtracting the CYP-HS from the CYP-RCPs. Figure 9 displays changes (RCPs minus HS) in the square mean differences of T_a and T_1 (TS_CYP), DS (DS_CYP), and CYP of the maximum CYP-HS heading date (4 August) under the RCP4.5 and RCP8.5 runs, respectively. Both of these runs show similar spatial distributions, but the differences are larger in the RCP8.5 run than in the RCP4.5 run. The TS_CYP increases in regions other than the northeastern region of the Korean Peninsula and the Primorsky area of Russia, and such increases are particularly large in the southeastern region of China, the southwestern region of the Korean Peninsula, and the coastal area of Japan. This is because temperatures in these regions rise above T_1. The 40-day accumulated precipitation in the RCP runs is simulated to increase in most domains compared with the HS run; however, the 40-day accumulated precipitation hours are projected to decrease in all domains (not shown). This result is the same as found in previous studies (e.g., Chen and Sun, 2013; Oh *et al.*, 2014; Hong and Ahn, 2015) that showed increases in precipitation intensity under future climate according to increases in precipitation and decreases in precipitation frequency. Thus, the DS_CYP increases in most domains because of the decrease in precipitation hours in RCP runs compared with the HS run. The DS_CYP is longer by at least 15 h compared with the HS run during the grain filling period for 40 days. According to the changes in these two variables, the CYP decreases in almost all regions except for the northeastern region of the Korean Peninsula and the Primorsky area of Russia. Therefore, if ears of rice come into on the maximum CYP-HS heading date, the rice productivity of the RCP4.5 and RCP8.5

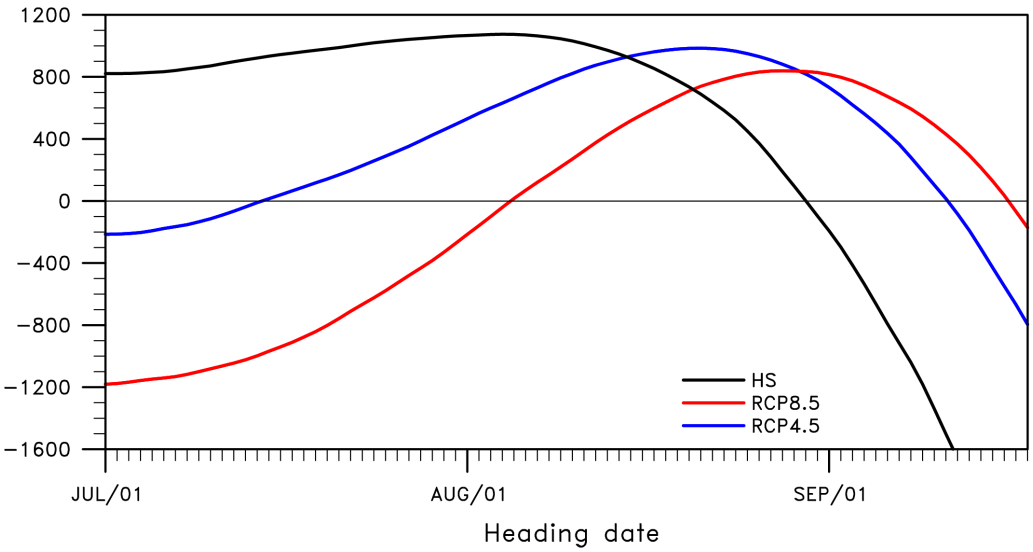

Figure 8. Domain area-averaged CYP with respect to heading date, for the HS, RCP4.5, and RCP8.5 runs.

runs would still be lower than that of the HS run in most regions.

Figure 10 illustrates the differences in TS_CYP, DS_CYP, and CYP, which are accumulated when the CYP is positive at individual grid points during the heading date period (1 July to 18 September) (CYP-RCPs$_{total}$ minus CYP-HS$_{total}$). As with Figure 9, the RCP4.5 and RCP8.5 runs exhibit similar distributions, but changes are more prominent in the RCP8.5 run. TS_CYP in the RCP4.5 run is seen to decrease a little in the northeastern region of the Korean Peninsula and in the Primorsky area of Russia, and then increases a little or shows no change in other regions. However, TS_CYP in the RCP8.5 increases in regions other than the northeastern region of the Korean Peninsula and the Primorsky area of Russia. DS_CYP of the RCP runs is seen to increase in comparison with that of the HS run in all domains, and in particular greatly increases in the southeastern region of China, the Primorsky area of Russia, and the central region of Japan. As a result in Figure 9, the CYP decreases in regions other than the northeastern region of the Korean Peninsula and the Primorsky area of Russia, and certain regions in Jilin region (125°–130°E, 42°–45°N) of China. In summary, rice productivity decreases in most regions that currently farm rice over a large area.

Therefore, in climates under the RCP4.5 and RCP8.5 runs, the optimum heading dates are projected to be delayed, and the periods during which heading would be possible are projected to be shortened in comparison with the HS run. In addition, the entire rice yield is projected to decrease because the accumulated CYP during the possible period of rice ripening, which the CYP exceeds 0, will greatly decrease in most regions.

5. Summary and discussion

Climate is one of the most important factors influencing agricultural production, and this paper therefore investigates agricultural climate change according to future climate change. In this study, the simulated future agro-climate indices mainly focused on rice production under RCP4.5 and RCP8.5 scenarios were compared with those of the present climate (Historical simulation), in order to investigate the possible changes in agricultural production in Northeast Asia. For this, a high-resolution regional climate of Northeast Asia was simulated by applying the low-resolution climate change scenario produced by HadGEM2-AO to WRF through dynamical downscaling. The WRF simulations were conducted from 1 January 1979 to 31 December 2010 for the HS run, and from 1 January 2019 to 31 December 2100 for the RCP4.5 and RCP8.5 runs to generate high space (12.5 km) and time resolution (1 h) data. Two different analysis periods were chosen to examine the agro-climate during different climatic periods: 1981–2010 for the current climate, and 2071–2100 for the future climate. The analysis variables used were daily mean surface air temperature, daily minimum temperature for frost days, hourly precipitation, and hourly incoming net shortwave. Using the dynamically downscaled high resolution data, agro-climates were analysed and projected in terms of the indices, such as vegetable and crop periods, frost days, and the CYP for Japonica type rice, one of the major crops presently cultivated in the Northeast Asia, where studies on the climate change-related rice production are rare.

According to our analysis, WRF simulates the general pattern and fine distributions of surface air temperature following terrain and altitude reasonably well in the HS run over Northeast Asia, resulting in good performance in producing fine-resolution frost days, vegetable and crop periods in the HS run similar to those in observation. Because of the increase in minimum temperature in this region, the number of frost days is projected to decrease by 19–30 days on average in RCP runs. Our results indicate that the 30-year mean vegetable periods are projected to be extended throughout MAMJJASO by 5–15 days and by

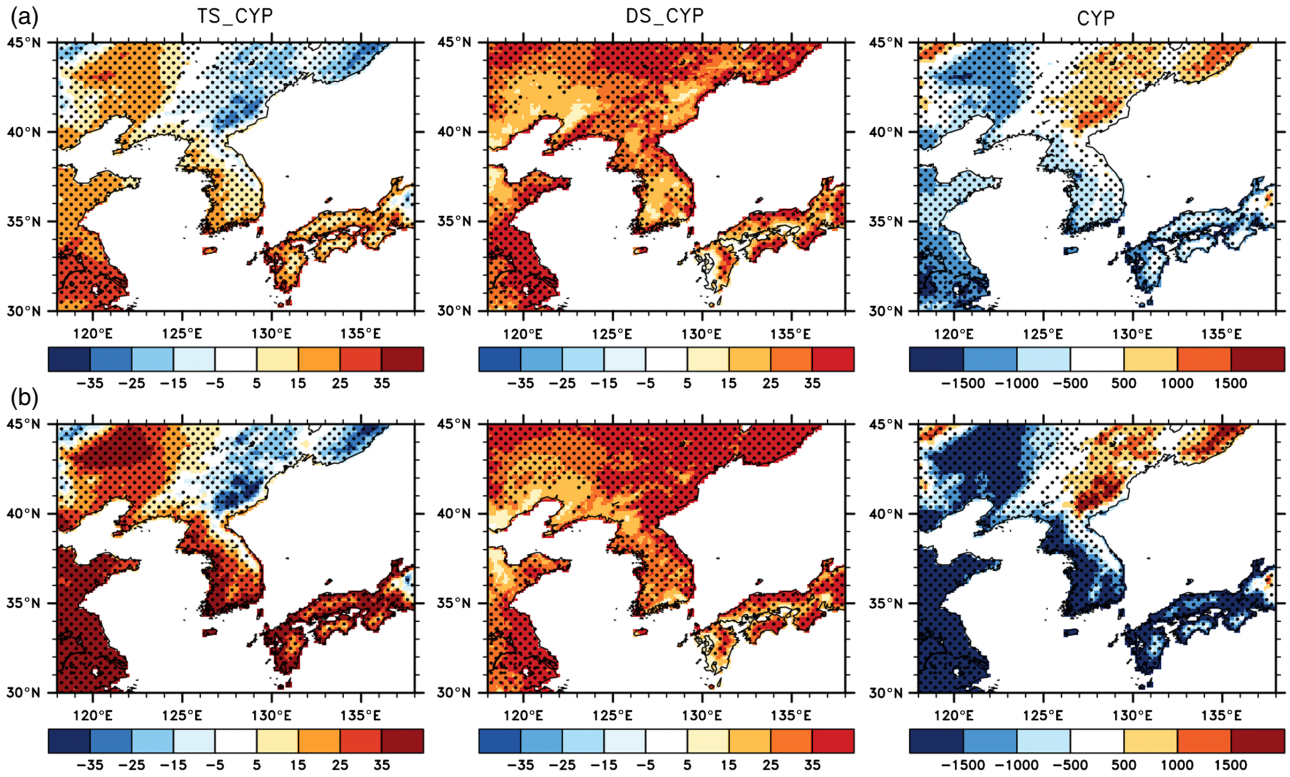

Figure 9. Changes in TS_CYP, DS_CYP, and CYP for: (a) RCP4.5 and (b) RCP8.5 runs against the maximum CYP-HS heading date (4 August). The panels on the far left shown the differences between the RCPs and the HS run for the square difference of surface air temperature and critical temperature averaged for the heading date. The middle panels represent the differences between the RCPs and HS runs for the 40-day accumulated duration of sunshine. The panels on the far right indicate the differences in the CYP between the RCPs and HS runs. Grid points with black dots show the 95% confidence level based on the Student's *t*-test.

10–35 days, for the RCP4.5 and RCP8.5 runs, respectively. The crop periods are also projected to increase by at least 10 days in both the RCP runs. These expected decreases in frost days and increases in growing periods are broadly consistent with previous studies focused on North America, Europe, West Africa, and South Asia (e.g., Heino *et al.*, 1999; Bonsal *et al.*, 2001; Frich *et al.*, 2002; Meehl *et al.*, 2004; Ramirez-Villegas *et al.*, 2013; Sillmann *et al.*, 2013; Sultan *et al.*, 2013; Maloney *et al.*, 2014; Yang *et al.*, 2014; Xia *et al.*, 2015). Whereas these studies used low-resolution model data, our results based on spatially and temporally high-resolution model data afforded a more detailed and comprehensive projection in terms of space and time.

Although improved agricultural conditions can be expected, the CYP is projected to decrease in relation to the increased temperature within the future climate, based on the RCP4.5 and RCP8.5 runs. This is projected to occur particularly in South Korea, Japan, and Southeast and Northeast China. Such a change is related to the projected temperature rise within these regions, which will exceed the grain-filling optimum temperature of rice. This implies that the CYP of RCPs for rice is set to decline in most regions, except for the north part of the Korean Peninsula and the Primorsky area of Russia, if the period of heading dates for rice is the same as the current period, because of the increase in temperature which exceeds the most favourable crop temperature. The result is roughly similar to the projection of Zhou and Wang (2015) who estimated a 14.83% increase of rice yields in northeastern China for the period 2070–2099 compared with the period 1976–2005 under the RCP4.5 scenario using a crop model with low-resolution global data.

The accumulated CYP where the CYP is higher than 0 in the RCP runs decreases compared with that of the HS run in the southern region of the Korean Peninsula and in Japan, where rice is currently produced in large quantities. The domain-averaged maximum CYP-RCPs decrease by 90–236 kg per unit area (1000 m^2) more than that of the CYP-HS. Both indicate that the average rice productivity is projected to decrease compared with that in the Historical climate. In addition, the number of days during which the rice ripening is possible is also expected to decrease. This implies that in climates under the RCP 4.5 and RCP8.5 scenarios, the cultivation of diverse cultivars of rice which have different heading dates will become difficult because of the reduction of the possible period of rice ripening. The future domain-average optimum grain-filling periods for rice are also expected to be delayed by 2–3 weeks compared with the present period. The agricultural environment that is currently suitable for the growth of rice is likely to deteriorate.

The limitations of this study include the lack of consideration for the development of varieties suitable for growth within this altered climate, or of biological changes associated with greenhouse gas increases (such as the overgrowth

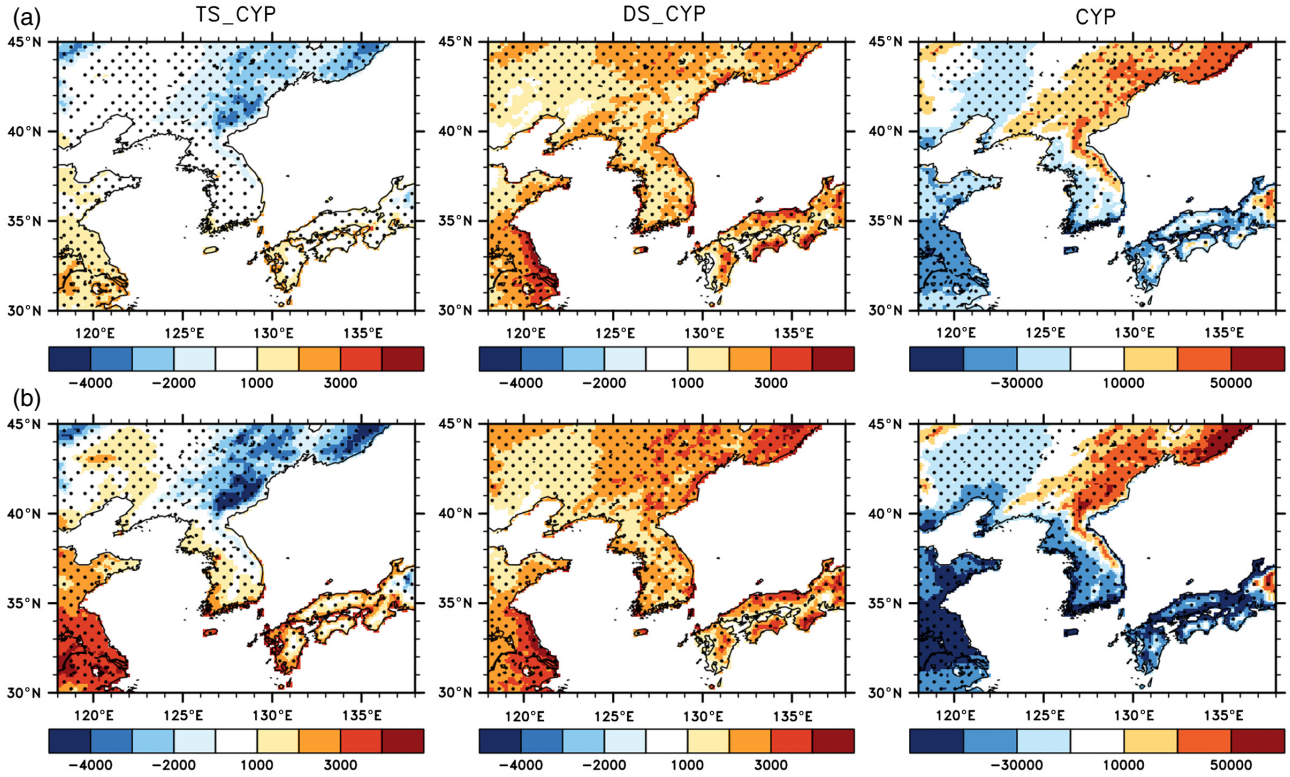

Figure 10. Same as Figure 9, except for accumulated data when values of CYP are above 0 for: (a) RCP4.5 and (b) RCP8.5 runs compared with the HS run.

of crops and vegetation in an environment with increased greenhouse gases). In addition, the effects of climatic damage have not been considered, such as the loss of crops in relation to extreme weather events. In addition, this study used only a single regional model with a boundary condition sourced from a single CMIP5 model for the projection of agro-climate changes. Further model studies using diverse CGCMs and RCMs may reduce the uncertainty of projection and reveal the range of the uncertainty.

Acknowledgements

This work was funded by the Korea Meteorological Administration Research and Development Program under grant KMIPA 2015-2081 and carried out with the support of Rural Development Administration Cooperative Research Program for Agriculture Science and Technology Development under Grant Project No. PJ009953. The authors wish to thank division of supercomputer management of the KMA for providing us with the supercomputer resources and consultations in relation to technical support.

References

Ahn JB, Lee J, Im ES. 2012. The reproducibility of surface air temperature over South Korea using dynamical downscaling and statistical correction. *J. Meteorol. Soc. Jpn.* **90**: 493–507, doi: 10.2151/jmsj.2012-404.

Alexandratos N, Bruinsma J. 2012. World agriculture towards 2030/2050: the 2012 revision. ESA Working paper No. 12-03, FAO, Rome.

Australian Agency for International Development. 2004. *Food Security Strategy*. Commonwealth of Australia: Canberra.

Baek HJ, Lee J, Lee HS, Hyun YK, Cho C, Kwon WT, Marzin C, Gan SY, Kim MJ, Choi DH, Lee J, Lee J, Boo KO, Kang HS, Byun YH. 2013. Climate change in the 21st century simulated by HadGEM2-AO under representative concentration pathways. *Asia-Pac. J. Atmos. Sci.* **49**: 603–618, doi: 10.1007/s13143-013-0053-7.

Bonsal BR, Zhang X, Vincent LA, Hogg WD. 2001. Characteristics of daily and extreme temperatures over Canada. *J. Clim.* **14**: 1959–1976, doi: 10.1175/1520-0442(2001)014<1959:CODAET>2.0.CO;2.

Central Intelligence Agency. 2014. *The World Factbook*. https://www.cia.gov/library/publications/the-world-factbook/rankorder/2119rank.html (accessed 20 February 2015).

Chen F, Dudhia J. 2001. Coupling an advanced land-surface/hydrology model with the Penn State/NCAR MM5 modeling system. Part I: model description and implementation. *Mon. Weather Rev.* **129**: 569–585, doi: 10.1175/1520-0493(2001)129<0569:CAALSH>2.0.CO;2.

Chen H, Sun J. 2013. Projected change in East Asian summer monsoon precipitation under RCP scenario. *Meteorol. Atmos. Phys.* **121**: 55–77.

Collins WD, Hackney JK, Edwards DP. 2002. An updated parameterization for infrared emission and absorption by water vapor in the National Center for Atmospheric Research Community Atmosphere Model. *J. Geophys. Res.* **107**: 1–20, doi: 10.1029/2001JD001365.

Collins WJ, Bellouin N, Doutriaux-Boucher M, Gedney N, Halloran P, Hinton T, Hughes J, Jones CD, Joshi M, Liddicoat S, Martin G, O'Connor F, Rae J, Senior C, Sitch S, Totterdell I, Wiltshire A, Woodward S. 2011. Development and evaluation of an Earth-system model – HadGEM2. *Geosci. Model Dev.* **4**: 997–1062, doi: 10.5194/gmd-4-1051-2011.

Frich P, Alexander LV, Della-Marta P, Gleason B, Haylock M, Klein Tank AMG, Peterson T. 2002. Observed coherent changes in climatic extremes during the second half of the twentieth century. *Clim. Res.* **19**: 193–212, doi: 10.3354/cr019193.

Gao C. 2012. The impact of climate change on China's crop production: a CMIP5 ensemble assessment. In *Proceeding of*

Agro-Geoinformatics 2012 Conference, Shanghai, China. doi: 10.1109/Agro-Geoinformatics.2012.6311641.
Gao XJ, Wang ML, Giorgi F. 2013. Climate change over China in the 21st century as simulated by BCC_CSM1.1-RegCM4.0. *Atmos. Oceanic Sci. Lett.* **6**: 381–386, doi: 10.3878/j.issn.1674-2834.13.0029.
Gerelchuluun B, Ahn JB. 2014. Air temperature distribution over Mongolia using dynamical downscaling and statistical correction. *Int. J. Climatol.* **34**: 2464–2476, doi: 10.1002/joc.3853.
Hanyu J, Uchijima T, Sugawara S. 1966. Studies on the agro-climatological method for expressing the paddy rice products. I. An agro-climatic index for expressing the quantity of ripening of the paddy rice. *Bull. Tohoku Natl. Agric. Exp. Stn.* **34**: 27–36.
Harris I, Jones PD, Osborn TJ, Lister DH. 2014. Updated high-resolution grids of monthly climatic observations – the CRU TS3.10 dataset. *Int. J. Climatol.* **34**: 623–642, doi: 10.1002/joc.3711.
Heino R, Brázdil R, Førland E, Tuomenvirta H, Alexandersson H, Beniston M, Pfister C, Rebetez M, Rosenhagen G, Rösner S, Wibig J. 1999. Progress in the study of climate extremes in northern and central Europe. *Clim. Change* **42**: 151–181, doi: 10.1023/A:1005420400462.
Hong JY, Ahn JB. 2015. Changes of early summer precipitation in the Korean Peninsula and nearby regions based on RCP simulations. *J. Clim.* **28**: 3557–3578, doi: 10.1175/JCLI-D-14-00504.1.
Hong SY, Dudhia J, Chen SH. 2004. A revised approach to ice microphysical processes for the bulk parameterization of clouds and precipitation. *Mon. Weather Rev.* **132**: 103–120, doi: 10.1175/1520-0493(2004)132<0103:ARATIM>2.0.CO;2.
Hong SY, Noh Y, Dudhia J. 2006. A new vertical diffusion package with an explicit treatment of entrainment processes. *Mon. Weather Rev.* **134**: 2318–2341, doi: 10.1175/MWR3199.1.
Jiménez PA, Dudhia J, González-Rouco JF, Navarro J, Montávez JP, García-Bustamante E. 2012. A revised scheme for the WRF surface layer formulation. *Mon. Weather Rev.* **140**: 898–918, doi: 10.1175/MWR-D-11-00056.1.
Kain JS. 2004. The Kain-Fritsch convective parameterization: an update. *J. Appl. Meteorol.* **43**: 170–181, doi: 10.1175/1520-0450(2004)043<0170:TKCPAU>2.0.CO;2.
Kim CS, Lee JS, Ko JY, Yun ES, Yeo US, Lee JH, Kwak DY, Shin MS, Oh BG. 2007. Evaluation of optimum rice heading period under recent climatic change in Yeongnam area. *Korean J. Agric. For. Meteorol.* **9**: 17–28.
Lal R, Uphoff N, Stewart BA, Hansen DO. 2005. *Climate Change and Global Food Security*. CRC Press: Boca Raton, FL.
Lee CK, Kim J, Shon J, Yang WH, Yoon YH, Choi KJ, Kim KS. 2012. Impacts of climate change on rice production and adaptation method in Korea as evaluated by simulation study. *Korean J. Agric. For. Meteorol.* **14**: 207–221, doi: 10.5532/KJAFM.2012.14.4.207.
Maloney ED, Camargo SJ, Chang E, Colle B, Fu R, Geil KL, Hu Q, Jiang X, Johnson N, Karnauskas KB, Kinter J, Kirtman B, Kumar S, Langenbrunner B, Lombardo K, Long LN, Mariotti A, Meyerson JE, Mo KC, Neelin JD, Pan Z, Seager R, Serra Y, Seth A, Sheffield J, Stroeve J, Thibeault J, Xie SP, Wang C, Wyman B, Zhao M. 2014. North American Climate in CMIP5 experiments: part III: assessment of twenty-first-century projections. *J. Clim.* **27**: 2230–2270, doi: 10.1175/JCLI-D-13-00273.1.
Meehl GA, Tebaldi C, Nychka D. 2004. Changes in frost days in simulations of twenty-first century climate. *Clim. Dyn.* **23**: 495–511, doi: 10.1007/s00382-004-0442-9.
Meehl GA, Covey C, Taylor KE, Delworth T, Stouffer RJ, Latif M, McAvaney B, Mitchell JFB. 2007. The WCRP CMIP3 multimodel dataset: a new era in climate change research. *Bull. Am. Meteorol. Soc.* **88**: 1383–1394, doi: 10.1175/BAMS-88-9-1383.
Meinshausen M, Smith SJ, Calvin KV, Daniel JS, Kainuma MLT, Lamarque JF, Matsumoto K, Montzka SA, Raper SCB, Riahi K, Thomson AM, Velders GJM, van Vuuren D. 2011. The RCP greenhouse gas concentrations and their Extension from 1765 to 2300. *Clim. Change* **109**: 213–241, doi: 10.1007/s10584-011-0156-z.
Moonen AC, Ercoli L, Mariotti M, Masoni A. 2002. Climate change in Italy indicated by agrometeorological indices over 122 years. *Agric. For. Meteorol.* **111**: 13–27, doi: 10.1016/S0168-1923(02)00012-6.
Moss R, Babiker M, Brinkman S, Calvo E, Carter T, Edmonds J, Elgizouli I, Emori S, Erda L, Hibbard K, Jones R, Kainuma M, Kelleher J, Lamarque JF, Manning M, Matthews B, Meehl J, Meyer L, Mitchell J, Nakicenovic N, O'Neill B, Pichs R, Riahi K, Rose S, Runci P, Stouffer R, van Vuuren D, Weyant J, Wilbanks T, van Ypersele JP, Zurek M. 2008. Technical summary. In *Towards New Scenarios for Analysis of Emissions, Climate Change, Impacts, and Response Strategies*. Intergovernmental Panel on Climate Change: Geneva, Switzerland.
Oh SG, Park JH, Lee SH, Suh MS. 2014. Assessment of the RegCM4 over East Asia and future precipitation change adapted to the RCP scenarios. *J. Geophys. Res. Atmos.* **119**: 2913–2927, doi: 10.1002/2013JD020693.
Organisation for Economic Co-operation and Development–Food and Agriculture Organization. 2013. *OECD-FAO Agricultural Outlook 2013*. OECD Publishing. doi: 10.1787/agr_outlook-2013-en.
Ramirez-Villegas J, Challinor AJ, Thornton PK, Jarvis A. 2013. Implications of regional improvement in global climate models for agricultural impact research. *Environ. Res. Lett.* **8**: 024018, doi: 10.1088/1748-9326/8/2/024018.
Shim KM, Kim GY, Roh KA, Jeong HC, Lee DB. 2008. Evaluation of agro-climatic indices under climate change. *Korean J. Agric. For. Meteorol.* **10**: 113–120.
Sillmann J, Kharin VV, Zwiers FW, Zhang X, Bronaugh D. 2013. Climate extremes indices in the CMIP5 multimodel ensemble: Part 2. Future climate projections. *J. Geophys. Res. Atmos.* **118**: 2473–2493, doi: 10.1002/jgrd.50188.
Skamarock WC, Klemp JB, Dudhia J, Gill DO, Barker DM, Duda MG, Huang XY, Wang W, Powers JG. 2008. A description of the advanced research WRF version 3. NCAR Technical Note, NCAR/TN-475+STR. Mesoscale and Microscale Meteorology Division, National Center for Atmospheric Research, Boulder, CO, USA. doi: 10.5065/D68S4MVH.
Son Y, Lee HW, Kim SY, Hwang DY, Park ST, Yang SJ. 2002. Relationship of climatic factors to rice yield in different area. Yeongnam Agricultural Research Institute research report 162-172, Yeongnam Agricultural Research Institute, Milyang, Korea. (in Korean with English abstract)
Su YY, Weng YH, Chiu YW. 2009. Climate change and food security in East Asia. *Asia-Pac. J. Clin. Nutr.* **18**: 674–678.
Sultan B, Roudier P, Quirion P, Alhassane A, Muller B, Dingkuhn M, Ciais P, Guimberteau M, Traore S, Baron C. 2013. Assessing climate change impacts on sorghum and millet yields in the Sudanian and Sahelian savannas of West Africa. *Environ. Res. Lett.* **8**: 014040, doi: 10.1088/1748-9326/8/1/014040.
Taylor KE, Stouffer RJ, Meehl GA. 2012. An overview of CMIP5 and the experiment design. *Bull. Am. Meteorol. Soc.* **93**: 485–498, doi: 10.1175/BAMS-D-11-00094.1.
U.S. Government. 2010. *Feed the future guide. Feed the future initiative*. http://feedthefuture.gov/sites/default/files/resource/files/FTF_Guide.pdf (accessed 29 September 2014).
van Vuuren DP, Edmonds J, Kainuma M, Riahi K, Thomson A, Hibbard K, Hurtt GC, Kram T, Krey V, Lamarque JF, Masui T, Meinshausen M, Nakicenovic N, Smith SJ, Rose SK. 2011. The representative concentration pathways: an overview. *Clim. Change* **109**: 5–31, doi: 10.1007/s10584-011-0148-z.
Wei X, Jiang L, Xu J, Zhang W, Lu G, Zhang Y, Wan J. 2008. Genetic analyses of heading date of Japonica rice cultivars from Northeast China. *Field Crop Res.* **107**: 147–154, doi: 10.1016/j.fcr.2008.01.008.
Wei XJ, Jiang L, Xu JF, Liu X, Liu SJ, Zhai HQ, Wan JM. 2009. The distribution of japonica rice cultivars in the lower region of the Yangtze River Valley is determined by its photoperiod-sensitivity and heading date genotypes. *J. Integr. Plant Biol.* **51**: 922–932, doi: 10.1111/j.1744-7909.2009.00866.x.
Xia J, Yan Z, Jia G, Zeng H, Jones PD, Zhou W, Zhang A. 2015. Projections of the advance in the start of the growing season during the 21st century based on CMIP5 simulations. *Adv. Atmos. Sci.* **32**: 831–838, doi: 10.1007/s00376-014-4125-0.
Yang S, Feng J, Dong W, Chou J. 2014. Analyses of extreme climate events over china based on CMIP5 historical and future simulations. *Adv. Atmos. Sci.* **31**: 1209–1220, doi: 10.1007/s00376-014-3119-2.
Yasutomi N, Hamada A, Yatagai A. 2011. Development of a long-term daily gridded temperature dataset and its application to rain/snow discrimination of daily precipitation. *Glob. Environ. Res.* **15**: 165–172.
Zhou M, Wang H. 2015. Potential impact of future climate change on crop yield in Northeastern China. *Adv. Atmos. Sci.* **32**: 889–897, doi: 10.1007/s00376-014-4161-9.